HHS Public Access

Author manuscript

Cell Rep. Author manuscript; available in PMC 2018 October 10.

Published in final edited form as:

Cell Rep. 2018 September 04; 24(10): 2709–2722. doi:10.1016/j.celrep.2018.07.096.

Rapid Assembly of Presynaptic Materials behind the Growth Cone in Dopaminergic Neurons Is Mediated by Precise Regulation of Axonal Transport

David M. Lipton[1,2], **Celine I. Maeder**[1], and **Kang Shen**[1,3,*]

[1]Howard Hughes Medical Institute, Department of Biology, Stanford University, 385 Serra Mall, Stanford, CA 94305, USA

[2]Neurosciences Program, Stanford University School of Medicine, Stanford, CA 94305, USA

[3]Lead Contact

SUMMARY

The proper assembly of neural circuits depends on the process of synaptogenesis, or the formation of synapses between partner neurons. Using the dopaminergic PDE neurons in *C. elegans*, we developed an *in vivo* system to study the earliest steps of the formation of *en passant* presynaptic specializations behind an extending growth cone. We find that presynaptic materials coalesce into puncta in as little as a few minutes and that both synaptic vesicle (SV) and active zone (AZ) proteins arrive nearly simultaneously at the nascent sites of synapse formation. We show that precise regulation of UNC-104/Kinesin-3 determines the distribution of SV proteins along the axon. The localization of AZ proteins to *en passant* puncta, however, is largely independent of the major axonal kinesins: UNC-104/Kinesin-3 and UNC-116/ Kinesin-1. Moreover, AZ proteins play a crucial role in recruiting and tethering SV precursors (SVPs).

In Brief

Lipton et al. explore the initial steps of synapse formation *in vivo*. They find that clustering of major presynaptic material occurs extremely rapidly (<5 min). Both synaptic vesicle precursors and active zone proteins accumulate simultaneously at developing puncta. Precise regulation of the Kinesin-3 activation state strongly influences the positioning of vesicles along the axon during development.

Graphical Abstract

*Correspondence: kangshen@stanford.edu.

AUTHOR CONTRIBUTIONS

Conceptualization, K.S. and D.M.L.; Methodology, K.S., D.M.L., and C.I.M.; Software, D.M.L.; Formal Analysis, D.M.L.; Investigation, D.M.L.; Writing – Original Draft, D.M.L.; Writing – Review & Editing, K.S., D.M.L., and C.I.M.; Resources, D.M.L. and C.I.M.; Supervision, K.S.; Funding Acquisition, K.S.

DECLARATION OF INTERESTS

The authors declare no competing interests.

SUPPLEMENTAL INFORMATION

Supplemental Information includes Supplemental Experimental Procedures and five figures and can be found with this article online at https://doi.org/10.1016/j.celrep.2018.07.096.

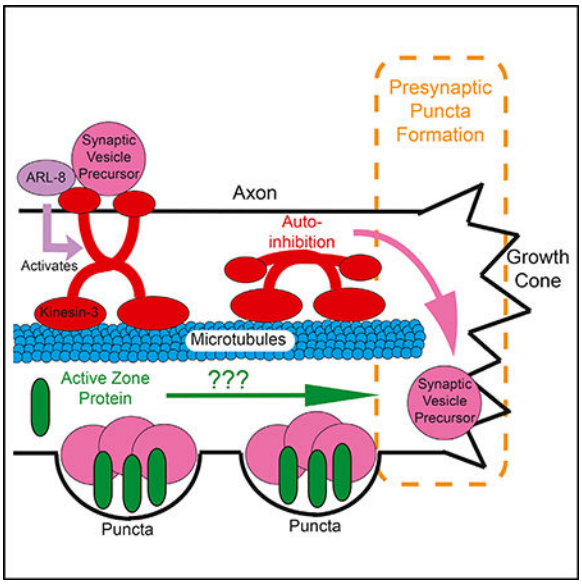

INTRODUCTION

The function of neural circuits depends on the precise assembly of synapses between appropriate partner neurons through the process of synaptogenesis. At a typical synapse, presynaptic specializations in the axon contain synaptic vesicles (SVs) and active zone (AZ) structures where neurotransmitter release takes place. AZ proteins dock and prime SVs for efficient release by positioning them close to the presynaptic membrane near calcium channels, and they coordinate the opposition of pre- and postsynaptic specializations via *trans*-synaptic cell-adhesion molecules (Petzoldt et al., 2016; Südhof, 2012). Although significant progress has been made in understanding the basic structure and components of the synapse, we still do not have a good understanding of how AZ molecules and SVs converge during synaptogenesis *in vivo*.

Several studies have taken a live imaging approach to characterize the process of synaptogenesis and the order of arrival of core components of the synapse. Using rodent hippocampal neuronal cultures, it has been observed that synapses are fed by VAMP-labeled SV transport packets (Ahmari et al., 2000), as well as traveling clusters of AZ proteins labeled by Bassoon (Friedman et al., 2000), followed by the recruitment of postsynaptic proteins and receptors (Friedman et al., 2000).

More recently, several studies have examined the molecular events underlying the synapse formation process *in vivo* (Böhme et al., 2016; Easley-Neal et al., 2013; Fouquet et al., 2009). In *C. elegans*, work from our lab and others has implicated the AZ proteins SYD-1 and SYD-2 as key players in recruiting other AZ proteins, as well as SVs, to the synapse (Dai et al., 2006; Patel et al., 2006; Zhen and Jin, 1999). At the *Drosophila* neuromuscular junction (NMJ), new synapses continually form in motor-neuron axon terminals. There, SYD-2/Liprin-alpha, SYD-1, and one isoform of UNC-13 arrive early in synapse development (Fouquet et al., 2009) (Böhme et al., 2016). Bruchpilot/ELKS-1, RIM binding protein, and a second UNC-13 isoform arrive later and are required for subsequent clustering

of calcium channels and presynapse maturation (Böhme et al., 2016; Fouquet et al., 2009). However, the earliest molecular events that lead to synapse formation behind an extending growth cone and how the various components of presynaptic terminals are supplied to synaptic sites are still not known.

To supply at least some of the crucial components of synapses, kinesin and dynein motors transport axonal cargoes along microtubules (Kevenaar and Hoogenraad, 2015; Maeder et al., 2014). SVs, which are thought to be first generated in the cell body, are transported as SV precursors (SVPs) by UNC-104/Kinesin-3 motors (Hall and Hedgecock, 1991; Okada et al., 1995; Pack-Chung et al., 2007) before pausing and accumulating at synaptic sites (Jin and Garner, 2008; Sabo et al., 2006). Studies from our lab show that the SV-bound small guanosine triphosphatase (GTPase) ARL-8 activates UNC-104/ Kinesin-3 and prevents its auto-inhibition to ensure the delivery of SVPs to the distal axon (Klassen et al., 2010; Wu et al., 2013). Yet it is not known how SVPs are deposited at nascent *en passant* presynaptic puncta as they are first forming behind an extending growth cone.

Like SVPs, AZ proteins are synthesized in the cell body (Dresbach et al., 2006; Maas et al., 2012). It has been proposed that they are incorporated into transport vesicles termed Piccolo-Bassoon transport vesicles (PTVs, named for the particular AZ components initially described) (Shapira et al., 2003; Zhai et al., 2001; Ziv and Garner, 2004). PTVs were observed transiting down the axon to sites of synapse assembly, where a relatively small number of mobile PTVs coalesced to form the AZ (Shapira et al., 2003). However, PTV transport packets have been difficult to observe *in vivo* (Petzoldt et al., 2016). In addition, there is no consensus about which motors are used for AZ protein transport, though Kinesin-3 and Kinesin-1 are the most likely candidates given their known important roles in axonal transport (Goldstein et al., 2008; Gumy et al., 2017; Hall and Hedgecock, 1991; Pack-Chung et al., 2007; Patel et al., 2006).

We developed an *in vivo* system to observe the initial steps of the *de novo* formation of *en passant* presynaptic specializations using the *C. elegans* PDE dopaminergic neuron. We chose to focus our efforts on this dopaminergic neuron for two reasons: (1) PDE axons grow out rapidly during postembryonic development, developing *en passant* presynaptic specializations along their entire axon lengths and making the key cellular processes underlying the early stages of synapse formation amenable to observation. (2) In vertebrates, dopamine release occurs via volume transmission, during which dopamine is diffusely released onto target brain regions from widely arborized terminals, many of which are not directly opposed to a postsynaptic density and spine (Sulzer et al., 2016; Trudeau et al., 2014). Because dopaminergic neurons can form synapses independently of a well-aligned postsynaptic partner, presynaptic assembly mechanisms likely play a central role in the formation of these unique synapses, which were only recently characterized (Liu et al., 2018).

Using this system, we find that dopaminergic PDE neurons develop clusters of AZ proteins along their axons. We also find that AZ proteins and SVPs coalesce into nascent synaptic puncta extremely rapidly behind the extending PDE growth cone—within several minutes. Following this initial phase of rapid puncta formation, there is a second phase of remodeling

and organization during which clusters of SVs and AZ proteins increase in size and stability. We find that transport of AZ proteins down the axon is mostly independent of UNC-104/Kinesin-3 and UNC-116/Kinesin-1. Finally, we show that de novo puncta formation depends on a proper balance between motor-driven transport and AZ protein-dependent aggregation.

RESULTS

Dopaminergic Presynaptic Specializations in PDE Contain AZ Proteins

The two bilaterally symmetric PDE dopaminergic neurons extend ciliated sensory endings into the cuticle and, along with the ADE and CEP dopamine neurons, mediate the basal slowing response behavior in which the worm slows upon contact with food (Sawin et al., 2000). In vertebrates, dopamine is often released diffusely, rather than onto precisely aligned opposing postsynaptic receptors (Sulzer et al., 2016; Trudeau et al., 2014). We sought to characterize whether PDE's synaptic structure is similarly arranged. PDE's main downstream synaptic partner is the DVA interneuron, which expresses the D1-like dopamine receptor DOP-1C (Bhattacharya et al., 2014). We expressed SNB-1::YFP presynaptically in PDE and tdTomato::DOP-1C postsynaptically in DVA. Whereas SNB-1::YFP formed discrete puncta along the PDE axon, tdTomato::DOP-1C was diffuse along the DVA neurite (Figures 1B and 1C).

The expression pattern of pre- and postsynaptic proteins suggested that PDE might release dopamine through volume transmission in a similar manner to vertebrate dopaminergic neurons and thus might be a good model for understanding dopaminergic synapse formation. The molecular composition of vertebrate dopaminergic presynaptic terminals has recently been reported (Liu et al., 2018), so we wanted to determine whether PDE dopamine neurons contain a similar complement of AZ proteins. We decided to look at the localization of AZ proteins SYD-2/Liprin-alpha, UNC-10/RIM, CLA-1/Piccolo, and ELKS-1 and determine whether they colocalized with SVs. SYD-2/Liprin-a is thought to be a key organizer of synapse assembly. It binds other AZ proteins and recruits both AZ proteins and SVs to the synapse (Dai et al., 2006; Kittelmann et al., 2013; Patel et al., 2006; Zhen and Jin, 1999). UNC-10/RIM has been shown to play a crucial role in binding and tethering vesicles and presynaptic calcium channels (Kaeser et al., 2011; Südhof, 2012). ELKS-1 is a synaptic scaffolding molecule that binds SYD-2 (Dai et al., 2006; Kittelmann et al., 2013) and UNC-10 (Wang et al., 2002) and helps recruit calcium channels to the synapse (Kittel et al., 2006). Finally, CLA-1 is a piccolo and bassoon-type scaffold molecule that recruits SVs to release sites (Xuan et al., 2017). To mark SVs, we used RAB-3, which is an abundant, small GTPase present on SVs that helps recruit vesicles to the synapse through interactions with RIM (Südhof, 2013).

We coexpressed GFP::ELKS-1 and tdTomato::RAB-3 in PDE neurons and found that in mature axons, both proteins formed discrete puncta with extensive colocalization (Figures 1D and 1E). Similarly, UNC-10/RIM::GFP and tdTomato::RAB-3 puncta showed a high degree of colocalization (Figure 1F). As expected, ELKS-1 and UNC-10 also colocalized well with each other (Figure 1G). The AZ components SYD-2 and CLA-1 formed puncta in PDE similar to ELKS-1 and UNC-10 (Figures 1H and 1I). To confirm that AZ proteins are endogenously expressed in PDE neurons, we tagged endogenous ELKS-1 in a cell-

typespecific manner using a conditional strategy based on flippase-mediated recombination (Schwartz and Jorgensen, 2016). Endogenous GFP::ELKS-1 puncta are clearly visible in the PDE axon (marked with cytosolic mCherry) (Figure 1J). Finally, we wanted to determine whether the RAB-3-labeled puncta correspond to dopamine-filled vesicles. We coexpressed the vesicular dopamine transporter CAT-1/VMAT::GFP and tdTomato::RAB-3 in PDE and found that they colocalized well with each other (Figure 1K). We concluded that similar to what has been found in vertebrate dopamine neurons (Liu et al., 2018), PDE dopamine axons contain specializations consisting of canonical AZ cytomatrix molecules and dopamine-filled vesicles.

SV and AZ Proteins Rapidly Coalesce behind the Growth Cone

Having observed that PDE neurons contain specializations of SVs and AZ proteins, we wanted to determine how these specializations first form behind the extending growth cone (Figures 2A and 2B). Shortly after PDE's neurogenesis, during larval stage L2, PDE extends its axon toward the ventral nerve cord (VNC), where it bifurcates. Its major branch turns anteriorly and grows within the VNC, elaborating approximately 40 *en passant* presynaptic specializations.

To observe how SVPs first aggregate at nascent synaptic specializations in PDE axons, we coexpressed both an SVP marker, GFP::RAB-3, and cytoplasmic mCherry under a dopamine neuron-specific promoter, *Pdat-1 (wyIs639)*, and imaged these transgenic worms at different time points of axon outgrowth (Figures 2C and 2D). These analyses showed that we can reliably detect GFP::RAB-3 puncta within a few microns of the tip of the growing axon, suggesting that SVPs coalesce at nascent synapses into puncta rapidly behind the growth cone (Figure 2D). To quantify the distribution of these puncta along the axon, we divided each PDE axon into 10 equal-length bins and computed the integrated puncta intensity of GFP::RAB-3 in each bin (Figure 2F). The intensity of GFP::RAB-3 at older, more proximal puncta was similar to the intensity at newer, more distal ones, except for a proximal zone of high intensity (Figure 2F). Moreover, as the animal aged, puncta intensity increased uniformly.

To confirm that our observations with the exogenously expressed transgenic array (*wyIs639*) reflected the endogenous RAB-3 distribution, we examined the endogenous RAB-3:: GFP distribution using a cell-type-specific endogenous GFP knockin strain (*ox699*), in which the endogenous GFP tag was expressed only upon addition of a cell-specific flippase (*Pdat-1*::flippase), as previously described (Figure 1J) (Schwartz and Jorgensen, 2016). We found that the endogenous RAB-3 distribution was similar to that of the transgene (Figures 2E and 2F). The intensity of the endogenous GFP::RAB-3 was comparable to transgenic GFP::RAB-3 (Figure 2F), indicating that we were not overexpressing the RAB-3 marker in our transgenic strain.

To track how AZ proteins accumulate in the growing axon, we expressed and imaged them throughout axon outgrowth. Prior studies have demonstrated that assembly-inducing AZ proteins such as Liprin-a/SYD-2 arrive early in the process of synapse formation (Böhme et al., 2016; Fouquet et al., 2009; Patel et al., 2006). Consistent with this idea, we found that in PDE, the AZ proteins ELKS-1::GFP, SYD-2/Liprin-α::GFP, and UNC-10/ RIM::GFP

rapidly coalesce into puncta at nascent synapses behind the growth cone (Figure S1). We therefore speculated that AZ aggregation might occur first and act to seed subsequent accumulation of SVPs.

To determine the time course and order in which SVPs and AZ proteins arrive at newly forming puncta, we imaged the rapid *de novo* aggregation of synaptic material in real time. We took time-lapse movies from transgenic worms expressing ELKS-1::GFP and TdTomato::RAB-3 (Figure 3A), imaging every minute, and generated kymographs to depict the change in localization of both tdTomato::RAB-3 and GFP::ELKS-1 over time (Figures 3B–3D). By tracking the leading edge of the axon on the kymograph, we calculated the rate of axon outgrowth to be up to 30 μm/hr, although it varied considerably. We found that GFP::ELKS-1 and tdTomato::RAB-3 cluster quickly behind the extending growth cone (Figures 3B–3D), in most cases forming puncta within minutes that were of comparable intensity to the puncta located in the most proximal region of the axon. In addition, we found that, surprisingly, both ELKS-1 and RAB-3 cluster simultaneously. UNC-10/RIM and RAB-3 behave similarly, coalescing and aggregating rapidly behind the growth cone (Figure S2). Thus, SVPs and AZ proteins simultaneously coalesce at nascent synapses behind the growth cone, suggesting a rapid nucleation event that recruits both essential components of presynaptic terminals.

To quantitatively characterize the time course of these puncta formation events and assess the variability of this process, we plotted the fluorescence intensity increase of puncta as they were developing. An example of such a formation event, demarcated by arrows, can be seen in the kymographs in each of the color channels and the composite image (Figures 3B–3D). To quantify the time course of puncta coalescence, we selected a punctum that had formed by the end of the movie and then traced it backward in time to create a vertical slice of the kymograph at that puncta's axonal location (correcting for any puncta movement). We then plotted the intensity changes over time in this vertical slice. A resultant plot of ELKS-1 and RAB-3 fluorescence intensity for one of these formation events reveals how quickly these puncta can form (Figure 3E). For the synaptic punctum depicted in Figures 3E, approximately 50% of its total intensity was gained in the first 2 min, with almost all remaining increase occurring in the next 15–20 min. We found considerable variability in the rate of puncta formation. Thus, to obtain an average rate of puncta formation, we averaged the fluorescence intensities of all newly forming puncta (by aligning fluorescence traces to the first fluorescence increase, which is indicative of growth cone arrival). In these mean fluorescence traces, we saw that both ELKS-1 and RAB-3 coalesce most rapidly in the first 5 min after the growth cone passes (Figure 3F). Then, there is a subsequent buildup over the next 10–15 min, completing this initial phase of assembly behind the growth cone.

To obtain movies with even greater temporal resolution of this aggregation process, we imaged the axon every 2.5 s for 15 min (Figure 3G). Again, we found rapid emergence of new ELKS-1 puncta, which formed within 1–2 min, demonstrating that the initial coalescence event from the diffuse pool of ELKS-1 occurred even faster than we could originally resolve with our longer, lower-resolution videos. The timescale of these events is significantly faster than what has been reported in previous observations of synapse formation (Easley-Neal et al., 2013; Fouquet et al., 2009; Friedman et al., 2000).

We noticed that many of these newly formed puncta were mobile, in contrast to the older puncta in the most proximal region of the axon that were less mobile and more stable in terms of their size and intensity, and the relative proportions of the AZ and SV markers. We therefore suspected there might be a second phase of puncta stabilization and consolidation following the initial rapid seeding events. We quantified the colocalization of ELKS-1 and RAB-3 puncta throughout development using thresholded steady-state images of axonal puncta during development, finding an initial phase of rapid colocalization followed by a second phase of maturation throughout L3, in which puncta continued to coalesce, stabilize, and grow (Figure 3H). Thresholded long-term imaging kymographs of both ELKS-1 and RAB-3 demonstrated this developmentally increasing colocalization as well (Figure S3).

AZ Proteins and SVs Exhibit Distinct Axonal Transport Dynamics

Having observed how rapidly both SVPs and AZ proteins coalesce behind the axon, we wanted to ask how both of these materials are supplied to the region behind the growth cone, where puncta are readily forming. To image SVP transport down the axon, we photo-bleached GFP::RAB-3 intensity either just behind the growth cone (Figure 4A) or along the most proximal region of the axon (Figure 4E) and subsequently imaged the transport of RAB-3-labeled vesicles into the specified region, using high-temporal-resolution streaming movies (imaging at 7.5 frames per second). Bidirectional vesicular transport events that sometimes paused briefly and then resumed moving were apparent in the proximal axon (Figure 4E). As the transport events moved into the region behind the growth cone, they paused more frequently (Figure 4I) and for longer durations (Figure 4J). We did not see direction reversals in the region behind the growth cone, suggesting that SVPs that make it to the end of the axon accumulate there and become available to join newly forming puncta.

To determine how AZ proteins were supplied to the region of rapid coalescence at nascent synapses, we took streaming time-lapse movies of ELKS-1, UNC-10, or SYD-2 tagged with GFP after first photo-bleaching (Figures 4B–4D and 4F–4H), as we had for RAB-3. Although AZ proteins have been proposed to be transported on PTVs (Shapira et al., 2003; Zhai et al., 2001) in a manner similar to SVPs, all the AZ proteins we analyzed had far fewer observable transport events compared to RAB-3, by at least an order of magnitude (Figures 4K–4L). There were some slight differences in trafficking parameters of the AZ proteins. For instance, SYD-2 transport events had longer run lengths compared to the other AZ proteins we examined (Figure S4). Overall, transport events for AZ proteins were infrequent compared to the number of SVP transport events.

This result suggested that AZ materials may be supplied to the nascent puncta forming behind the growth cone by means other than fast axonal transport. We re-examined our ELKS-1 long-term imaging kymographs and found that in almost every kymograph, there were several slow anterograde movements of large ELKS-1 puncta (example shown in Figure 4M). These movements were heavily biased toward the anterograde direction and occurred most frequently in the region directly behind the growth cone (Figure 4M). These GFP::ELKS-1 movements were slow, around 0.01 mm/s, which is two orders of magnitude slower than the speeds typical of vesicular transport (1–2 mm/s). In the high-temporal-resolution (7.5 frames per second) movies of ELKS-1 (Figure 4F), we observed rare

transient anterograde movements of high fluorescence intensity followed by long pauses. These stop-andgo transient high-intensity movements, which were significantly faster than 0.01 mm/s (but less than velocities typical of vesicle transport), if averaged over long intervals, could correspond to the slow movements we observed in the long-term kymographs (1 image per minute). Crucially, these slow anterograde-biased movements do not feed the aggregating puncta at the axon tip, as SVP transport events do (Figure 4A). Rather, new ELKS-1 puncta mostly aggregate from a diffuse pool behind the growth cone tip and then are subsequently capable of engaging in these slow movements. Our observations of this slow type of transport are not limited to ELKS-1; we observed a similar phenomenon with UNC-10::GFP (Figure S3C).

Balance between SVP Transport and AZ Protein-Induced Aggregation Positions SV Clusters

To determine what cell biological and molecular mechanisms underlie the fast SVP and slow AZ protein transport events we observed and how these transport mechanisms influence the development of newly forming presynaptic puncta, we examined SVP and AZ puncta distribution in known transport mutants during early stages of PDE axon outgrowth. Mutants of either *unc-104/kinesin-3* or its upstream activator, *arl-8*, have previously been shown to disrupt SV distribution in adult worms: loss-of-function mutants result in a proximal shift of synaptic puncta, while kinesin overactivation leads to the formation of smaller synapses (Klassen et al., 2010; Niwa et al., 2016; Wu et al., 2013). Loss of the AZ protein *syd-2*, which is known to recruit additional presynaptic proteins, has also been shown to result in a reduction in the number and size of SV clusters and their dispersal into normally asynaptic regions (Klassen et al., 2010; Wu et al., 2013). In mutants of *arl-8*, an activator of kinesin-3, large ectopic clusters of SVPs form in the proximal axon, a phenotype that can be suppressed by either *unc-104/kinesin-3* overactivation or *syd-2* loss of function (Klassen et al., 2010; Wu et al., 2013). Altogether, these data have led to a model in which motor-driven transport works antagonistically with synapse assembly-promoting AZ proteins to control vesicle aggregation and synapse formation (Klassen et al., 2010; Maeder et al., 2014; Wu et al., 2013). However, the extent to which these mechanisms contribute to the initial stages of synapse formation had thus far been unexplored.

We first asked how reducing the strength of motor-driven transport by loss of the *unc-104/kinesin-3* activator, *arl-8*, would affect the deposition of SVPs at puncta along the developing axon. In wild-type early larval (L2 and early-L3) worms, both the SV protein RAB-3 and the AZ protein ELKS-1 are evenly distributed along the axon. Loss of *arl-8* resulted in RAB-3 accumulation in the most proximal regions of the axon, concomitant with a loss of RAB-3 puncta in the middle and distal axonal regions (Figures 5C and 5I). However, the distribution of ELKS-1 was unchanged in *arl-8* mutants (Figures 5D and 5J), suggesting that AZ proteins such as ELKS-1 do not require ARL-8-mediated UNC-104/Kinesin-3 transport.

In the *unc-104/kinesin-3* overactivation mutant (*wy673*), in which auto-inhibition is prevented (Niwa et al., 2016), RAB-3 puncta were dramatically reduced at proximal and medial regions along the axon and instead accumulated at the tip of the axon (Figures 5E and 5I). This severe phenotype suggests that the auto-inhibition of UNC-104 is a regulatory

mechanism that is essential for the formation of *en passant* RAB-3 puncta along the PDE axon. This overactive *kinesin-3* mutant had no effect on ELKS-1 distribution (Figures 5F and 5J), arguing that ELKS-1 proteins do not depend on regulation of Kinesin-3 activity for transport along the axon.

Having observed that the motor-activation state affected RAB-3 puncta distribution along the axon, we wanted to determine how loss of molecules that play a known role in SVP clustering would affect the formation of RAB-3 puncta. The AZ protein SYD-2/Liprin-alpha, upon activation by SYD-1, can recruit SVs to the synapse (Dai et al., 2006; Patel et al., 2006). To determine whether these AZ proteins might recruit transiting SVPs, as well as other AZ components, to the nascent puncta in PDE, we first analyzed puncta distribution in syd-2/liprin-alpha loss-of-function mutants at early larval stages (L2 and early-L3). Loss of SYD-2/Liprin-alpha resulted in a reduction of RAB-3 intensity at puncta along most of the axon, except for the most distal segments, where RAB-3 molecules instead accumulated (Figures 5G and 5I). *Syd-1*; *syd-2* double mutants exhibited a phenotype similar to that of *syd-2* single mutants (Figures 5I and 5J). In *syd-2* single mutants and *syd-1*; *syd-2* double mutants, ELKS-1 intensity slightly increased in the distal axon in L2 and early-L3 worms (Figures 5H and 5J). This increase was transient, however; in L4 worms, the distal puncta contained amounts of ELKS-1 similar to those found in wild-type controls (Figure 5L). Thus, whereas manipulations of both motor-driven transport and known SV-recruiting AZ proteins affected the distribution of SVPs along the axon, ELKS-1 localization was unaffected by either manipulation.

Because both the kinesin activation state and the AZ proteins SYD-1 and SYD-2/Liprin-alpha affect SVP distribution, we set out to determine whether one pathway was downstream of the other. To do so, we made double mutants between members of the two pathways (arl-8 and syd-2) and looked to see whether loss of one could suppress the phenotype of the other. In *arl-8*; *syd-2* double mutants, the distribution of RAB-3 was shifted more distally compared to the *arl-8* single mutant alone and was more evenly dispersed along the axon compared to the distal accumulation in *syd-2* single mutants (Figure 5I), suggesting that motor-driven transport and pro-assembly AZ molecules have the same net effect on SVPs: they determine the size and number of vesicle clusters along the axon. Reducing the strength of either of these two opposing pathways can compensate for loss of the other. Again, ELKS-1 localization was unaffected in these double mutants (Figure 5J).

We observed almost identical phenotypes between L2 and early-L3 worms and L4 worms for SV protein distribution (Figures 5I and 5K). This suggests that the same transport and SV-clustering mechanisms operate both during *de novo* puncta formation during development and during later puncta growth and maturation.

UNC-104/Kinesin-3 Activation State Dynamically Regulates SVP Transport

To gain more insight into how AZ proteins and motor-driven transport coordinate the distribution of SV cargoes in a developmental context, we measured the dynamic movement behavior of SVPs using GFP::RAB-3 in wild-type and mutant L3 worms. A region in the proximal PDE axon was photo-bleached to reduce background fluorescence and then

imaged continuously at a rate of 7.5 frames per second to visualize SVP transport events. Measurements of SVP pausing frequency and duration were calculated from kymographs.

We found that in *arl-8* mutants, SVP transport event frequency was dramatically reduced (Figures 6C and 6E), as were anterograde velocities (Figure 6G). There was also an increase in pause time (Figure 6K). These altered SVP dynamics explain the lack of vesicle clusters in the distal axon of *arl-8* mutants and argue that ARL-8 is required to activate UNC-104/Kinesin-3-mediated axonal transport of SVPs when synaptic puncta are first forming. Consistent with this idea, overactivating Kinesin-3 motor transport efficacy with a gain-of-function mutation resulted in increased anterograde run length, suggestive of a defect in the ability to capture transiting SVPs (Figure 6I). In addition, *unc-104* gain-of-function mutants had fewer retrograde transport events (Figure 6F), indicative of a disrupted balance between anterograde and retrograde SVP transport.

In *syd-1; syd-2* double mutants, mean anterograde run length, transport velocity, and pause time of SVP transport events were all unaffected (Figures 6G, 6I, and 6K). We have previously observed increased SVP transport event frequencies in *syd-2* (*wy5*) single mutants in another neuron, DA9 (Wu et al., 2013), an effect that could be masked in PDE (Figure 6E) due to the decrease in overall numbers of SVP events in this neuron, because synapses are smaller in PDE. Altogether, these data on SVP transport suggest that regulation of the activation state of UNC-104/Kinesin-3 by ARL-8 and Kinesin-3's auto-inhibitory mechanism is necessary to supply SVPs for initial clustering. Meanwhile, SYD-1 and SYD-2 recruit transiting SVPs without directly affecting the activation state of UNC-104/Kinesin-3.

AZ Protein Transport Is Mostly Independent of UNC-104/Kinesin-3 and UNC-116/Kinesin-1

Having observed different trafficking dynamics for AZ proteins compared to SVPs (Figure 4), we asked whether AZs and SVPs used different molecular mechanisms for axonal trafficking. It is known that SVPs depend on UNC-104/Kinesin-3 for their transport to synapses (Hall and Hedgecock, 1991; Okada et al., 1995). However, it is still largely unknown how AZ proteins are transported to the synapse, with conflicting evidence for their dependence on kinesin motors, particularly Kinesin-3 and Kinesin-1 (Goldstein et al., 2008; Klassen et al., 2010; Pack-Chung et al., 2007; Patel et al., 2006). AZ transport has been suggested to depend on Kinesin-3 at certain stages of development (Pack-Chung et al., 2007), but there is more recent evidence that this effect is indirect (Li et al., 2017). Thus, we wanted to ask how AZ protein distribution is affected by loss of *unc-104/kinesin-3* and *unc-116/kinesin-1* in PDE neurons when AZ protein clusters are first forming.

Whereas SVP puncta distribution was greatly perturbed by loss of function of *unc-104/kinesin-3*, as evidenced by loss of RAB-3 in the distal axon (Figures 7A and 7B), ELKS-1 puncta distribution was largely unaffected in *unc-104/kinesin-3* mutants (Figures 7A and 7C). SYD-2/Liprin-alpha::GFP was also *unc-104* independent (Figure 7D). In contrast, UNC-10/RIM showed a partial dependence on UNC-104/Kinesin-3. In wild-type worms, UNC-10/RIM exhibits a mild proximal-to-distal distribution gradient. This gradient was exacerbated in *unc-104/kinesin-3* mutant worms (Figure 7E), though the phenotype was not as severe as what is observed for the SVP marker RAB-3 (Figure 7B). These data indicate

that different AZ proteins may differentially depend on UNC-104/Kinesin-3 for transport, but that in PDE, all AZ proteins are either partially or completely independent of UNC-104/Kinesin-3.

Similarly, we found that most AZ proteins appeared to be independent of Kinesin-1. The proximal-distal distribution of the AZ marker ELKS-1 was unaffected in *unc-116/kinesin-1* worms (Figure 7F), as was SYD-2 (data not shown). SVP localization was also unaffected in *unc-116/kinesin-1* mutants (Figure 7G). In cultured vertebrate neurons, transport of dense core vesicles was observed by both Kinesin-3 and Kinesin-1, with distinct axon segments exhibiting different degrees of reliance on each of these motors (Gumy et al., 2017). We thus wanted to determine whether these two kinesin motors could function redundantly in transporting AZ proteins. We looked at ELKS-1 localization in *unc-104/kinesin-3; unc-116/kinesin-1* double mutants and observed that even in the double mutants, ELKS-1 localizes along the entire length of the axon (Figure S5).

To determine whether the low-frequency, slow anterograde movements of GFP::ELKS-1 puncta along the PDE axon (Figure 4) depended on *unc-104/kinesin-3 (e1265)* or *unc-116/kinesin-1* (*e2310*), we took long-term movies of synapse formation in these mutants (Figures 7H and 7I). GFP::ELKS-1 transport events were present in both kinesin mutants, suggesting that they are not mediated by Kinesin-3 or Kinesin-1.

DISCUSSION

How AZ components and SVs assemble into presynaptic terminals is an important question in neuronal cell biology, because the assembly of presynaptic specializations at specific locations in the nervous system instructs neural circuit assembly. However, the molecular mechanisms of *en passant* synapse formation *in vivo* have remained elusive, and few studies have observed the process of *de novo* synapse formation in real time during development.

Tracking this developmental process *in vivo*, we find that the initial stages of synapse formation, characterized by the rapid and convergent aggregation of SVPs and AZ proteins behind the developing growth cone, occur in as little as a few minutes (Figures 2 and 3). These puncta nucleation events spontaneously emerge out of a diffuse pool of AZ proteins (Figure 3) and SVPs. For SVPs, Kinesin-3-driven active transport events supply the materials necessary for presynaptic puncta formation behind the growth cone (Figure 4). After the initial puncta formation events, there is a subsequent phase of consolidation and stabilization, characterized by a continued increase in the amount of AZ proteins and SVs present, increased colocalization of AZ and SV markers, and increased stability of puncta positioning (Figures 2 and 3).

Although it has long been known that SVPs require UNC104/Kinesin-3 for transport to synapses (Hall and Hedgecock, 1991; Okada et al., 1995; Pack-Chung et al., 2007), it is not clear how vesicle transport is regulated to deposit SVPs at nascent synapses. We find that three intracellular processes must occur to appropriately distribute transported SVs at *en passant* sites along the axon. First, the UNC-104/Kinesin-3 motor must be activated by ARL-8 to ensure transport along the axon (Figures 5 and 6). Second, the kinesin motor is

auto-inhibited (Figures 5 and 6) (Niwa et al., 2016), allowing the transported cargoes to pause when the Kinesin-3 motor has been switched to the off state. Finally, pro-assembly AZ molecules capture and retain transiting SVPs at specific sites along the axon (Figure 5).

As the growth cone extends, we find that SVPs are continually supplied to previously formed synaptic puncta along the axon (Figures 5 and 6) and simultaneously deposited at nascent-forming puncta just behind the growth cone tip (Figure 4). Precise regulation of transport along the axon (Figures 5 and 6), combined with an overabundance of pausing at microtubule ends (Yogev et al., 2016), particularly in the coalescence region behind the growth cone (Figure 4), could ensure both the rapid puncta formation events (Figure 3), and the even distribution of vesicles among more mature *en passant* specializations. As the puncta transition from being newly coalesced at the growth cone tip to more mature ones along the axon undergoing consolidation and stabilization and further growth, they transition from being fed by the pool of SVPs arriving at the growth cone tip to being supplied by the pool of transiting SVPs moving bidirectionally along the axon (Figure 4). Manipulations of the strength of Kinesin-3 had a dramatic effect on puncta distribution along the axon. Overactivating the Kinesin-3 motor by disrupting auto-inhibition resulted in a dramatic loss of SVs at all AZ protein clusters along the axon. This highlights the specific importance of anterograde transport regulation for the earliest stages of synapse assembly.

AZ proteins also play an important role in clustering SVs: loss of the AZ protein SYD-2 causes a dramatic reduction of SVP accumulation at *en passant* sites, accompanied by accumulation toward the distal axon tip (Figure 5). Loss of *syd-2* and/ or *syd-1* could result in transiting SVPs bypassing their targets and accumulating at the nearest downstream location to which motor-driven transport carries them. These data suggest a model of synapse formation in which, after the initial rapid aggregation of synaptic material behind the growth cone, the maintenance of synapses is influenced by bidirectional motor-driven SVP transport (Figures 4 and 5). The bidirectional mobilization of synaptic material between synapses is similar to what has been observed for DCV trafficking in *Drosophila* motoneurons (Wong et al., 2012), as well as our findings from other neurons in *C. elegans* (Patel et al., 2006; Wu et al., 2013). In addition, these results from PDE show that similar SVP trafficking mechanisms function at both mature synapses in adult neurons and early in development, during the early stages of presynapse assembly.

In contrast to SVs, how individual AZ proteins travel to the synapse is less well understood (Petzoldt et al., 2016). Overall, our data on AZ localization and transport point toward the possibility that different AZ molecules use different mechanisms for transport to the synapse. The specific modes of transport for each of the AZ molecules might be determined by their position and function within the complex set of interactions that form the AZ. For instance, UNC-10/RIM, which binds more directly to SVs through direct interactions with RAB-3 (Petzoldt et al., 2016; Südhof, 2012), exhibited some slight dependence on UNC-104/Kinesin-3 for localization to the synapse. These UNC-10/RIM molecules may be hitching a ride on SVs, as has been observed for synapsin-I in hippocampal neurons (Scott et al., 2011; Tang et al., 2013). Cotrafficking has also been observed between SVs and AZ proteins in cultured hippocampal neurons (Tao-Cheng, 2007) and the *C. elegans* DA9 neuron (Wu et al., 2013).

However, both SYD-2 and ELKS-1 localized independently to puncta along the length of the axon of UNC-104/Kinesin-3 and UNC-116/Kinesin-1 in PDE neurons (Figure 7), and all manipulations of Kinesin-3 efficacy, which dramatically altered SV localization patterns, left ELKS-1 puncta mostly indistinguishable from wild-type (Figure 5). Furthermore, despite the rapidity with which AZ molecules such as ELKS-1 accumulated at nascent synapses in PDE, very low frequencies of AZ protein movements were observed (Figure 4). These infrequently observed transport events are likely insufficient to account for the rapid accumulation of AZ molecules at nascent synapses, because the slow transport events we did observe do not directly feed the puncta coalescing behind the growth cone. Instead, ELKS-1 seems to aggregate from a pool of diffuse material. It is possible that these AZ transport packets in PDE neurons contain few copies of AZ proteins; thus, observation of most transport events (including those feeding the puncta formation events) might require a more sensitive method of detection. We do observe rare, faint transport events for AZ proteins (Figure 4). However, AZ proteins still reach the synapse in mutants of the major axonal kinesins, Kinesin-1 and Kinesin-3 (Figures 5 and 7), which suggests that they do not rely on canonical motor-based transport.

A *priori*, diffusion is the most likely mode by which cytosolic AZ proteins could travel down the axon and supply material for the coalescence events in the axon tip. Nevertheless, the anterograde displacements of large ELKS-1 puncta that we observed (Figures 4 and 7), which were independent of Kinesin-1 and Kinesin-3 (Figure 7), could represent a possible mechanism for the bulk flow of ELKS-1 from the soma to the growing axon. It is conceivable that these large anterogradely moving ELKS-1 puncta could then disperse and thus contribute to the overall anterograde flux of ELKS-1, which could supply coalescence events behind the growth cone.

AZ proteins could also have dominant and secondary modes of transport. Vesicle-like movements were observed for SYD-2 (Figure 4); however, SYD-2 still clustered along the axon normally in *unc-104/kinesin-3* mutants (Figure 7), suggesting that SYD-2 might be capable of both vesicular and non-vesicular transport.

Regardless of how AZs are transported down the axon, they localize in evenly dispersed *en passant* synaptic puncta independent of the early arriving, vesicle-clustering AZ SYD-2/Liprin-alpha (Böhme et al., 2016; Fouquet et al., 2009; Patel et al., 2006), as ELKS-1 localization is largely unaffected in syd-2 mutants (Figure 5). This suggests the existence of upstream intracellular signals, which induce AZ aggregation.

In summary, we have established a model system for examining the early steps of *de novo* synaptogenesis of *en passant* dopamine synapses along an axon *in vivo*. We characterized the molecular composition of PDE dopaminergic presynaptic puncta and found that they are composed of many canonical AZ proteins that are colocalized with SV puncta. We also found that PDE coalescence events occur rapidly, in as little as a few minutes. We show that the proper regulation of Kinesin-3-mediated axonal transport and the action of synapse-assembly-promoting AZ molecules are necessary to appropriately deposit SVPs at nascent *en passant* puncta during development. Finally, we show that although SVPs highly depend

on Kinesin-3 transport mechanisms for travel along the axon, most AZ proteins travel from the cell body to the synaptic sites in PDE neurons largely by other means.

EXPERIMENTAL PROCEDURES

C. elegans Strains and Maintenance

C. elegans strains were maintained according to standard methods, as previously described. Strains were maintained at 20°C on plates seeded with OP50 strain *E. coli* bacteria. See Supplemental Experimental Procedures for strains used in study.

Imaging and Micrograph Generation

For all imaging experiments, imaging was performed using a Zeiss Observer.Z1 spinning disk confocal microscope and a Hamamatsu C9100–13 electron microscopy-charge-coupled device (EM-CCD) camera with a Zeiss 40×/1.3 or Zeiss 63×/1.4 objective. Images and videos were recorded using Metamorph Imaging software (Molecular Devices). Worms were immobilized by incubation with paralytics (levamisole plus 2,3-butanedione monoxime for steady-state images, levamisole for long-term time-lapse imaging, or muscimol for short-term time-lapse imaging of transport). Images were processed using ImageJ and/or MATLAB to isolate axon and generate kymographs. Details are in Supplemental Experimental Procedures.

Experimental Design and Statistical Analysis

Data were analyzed and figures were generated subsequently using MATLAB or GraphPad Prism. For Figure 2F, one-way ANOVA was run separately for *ox699* and *wyIs639*. Subsequent Tukey's tests showed no significant differences each of bins 5–9 compared to bin 1. For Figure 3H, GFP::ELKS-1 and tdTomato::RAB-3 colocalization was calculated by computing the percentage of thresholded ELKS-1 pixels along the axon that overlapped with thresholded RAB-3 pixels or as a negative control an x direction-shifted RAB-3 image. A two-way ANOVA was performed in GraphPad Prism, followed by Tukey's multiple comparison tests to compare individual age cohorts. For all panels in Figure 4, either a one-way ANOVA test (Figures 4I and 4J) or a Kruskal-Wallis test (Figures 4K and 4L) was used, depending on whether a Gaussian distribution of the data was assumed. Subsequently, Dunnett's multiple comparison test was used to determine significant differences between each of the mutant genotypes and the wild-type control. For Figures 5I–5L, a one-way ANOVA test was performed followed by multiple comparison Tukey's honest significant difference (h.s.d.) test. Tukey's h.s.d. test was used to compare each of bins 2–10 compared to bin 1 for a given genotype. Significance values are computed only within a genotype cohort. For Figures 6E–6L, significance was determined by a one-way ANOVA test (Figures 6E–6H) or a Kruskal-Wallis test (Figures 6I–6L), followed by Dunnett's multiple comparison test to compare mutant genotypes to wild-type. For Figure 7, one-way ANOVA followed by multiple comparison Tukey's h.s.d. test was performed in MATLAB. Significance values are computed within a genotype cohort.

Supplementary Material

Refer to Web version on PubMed Central for supplementary material.

ACKNOWLEDGMENTS

This work was supported by the Howard Hughes Medical Institute and the NIH (K.S.) (NIH NS103037 and NS091144). We would like to thank Peri Kurshan and Claire Richardson in the Shen lab for careful reading of this manuscript and for the insightful suggestions they and other members of the Shen lab provided. We would also like to thank Matthew Schwartz and the Jorgensen lab for providing reagents (ox699 and the SapTrap kit)

REFERENCES

Ahmari SE, Buchanan J, and Smith SJ (2000). Assembly of presynaptic active zones from cytoplasmic transport packets. Nat. Neurosci 3, 445–451. [PubMed: 10769383]

Bhattacharya R, Touroutine D, Barbagallo B, Climer J, Lambert CM, Clark CM, Alkema MJ, and Francis MM (2014). A conserved dopamine-cholecystokinin signaling pathway shapes context-dependent Caenorhabditis elegans behavior. PLoS Genet 10, e1004584. [PubMed: 25167143]

Böhme MA, Beis C, Reddy-Alla S, Reynolds E, Mampell MM, Grasskamp AT, Lützkendorf J, Bergeron DD, Driller JH, Babikir H, et al. (2016). Active zone scaffolds differentially accumulate Unc13 isoforms to tune Ca(2+) channel-vesicle coupling. Nat. Neurosci 19, 1311–1320. [PubMed: 27526206]

Dai Y, Taru H, Deken SL, Grill B, Ackley B, Nonet ML, and Jin Y (2006). SYD-2 Liprin-alpha organizes presynaptic active zone formation through ELKS. Nat. Neurosci 9, 1479–1487. [PubMed: 17115037]

Dresbach T, Torres V, Wittenmayer N, Altrock WD, Zamorano P, Zuschratter W, Nawrotzki R, Ziv NE, Garner CC, and Gundelfinger ED (2006). Assembly of active zone precursor vesicles: obligatory trafficking of presynaptic cytomatrix proteins Bassoon and Piccolo via a trans-Golgi compartment. J. Biol. Chem 281, 6038–6047. [PubMed: 16373352]

Easley-Neal C, Fierro J, Jr., Buchanan J, and Washbourne P (2013). Late recruitment of synapsin to nascent synapses is regulated by Cdk5. Cell Rep. 3, 1199–1212. [PubMed: 23602570]

Fouquet W, Owald D, Wichmann C, Mertel S, Depner H, Dyba M, Hallermann S, Kittel RJ, Eimer S, and Sigrist SJ (2009). Maturation of active zone assembly by Drosophila Bruchpilot. J. Cell Biol 186, 129–145. [PubMed: 19596851]

Friedman HV, Bresler T, Garner CC, and Ziv NE (2000). Assembly of new individual excitatory synapses: time course and temporal order of synaptic molecule recruitment. Neuron 27, 57–69. [PubMed: 10939331]

Goldstein AYN, Wang X, and Schwarz TL (2008). Axonal transport and the delivery of pre-synaptic components. Curr. Opin. Neurobiol 18, 495–503. [PubMed: 18950710]

Gumy LF, Katrukha EA, Grigoriev I, Jaarsma D, Kapitein LC, Akhmanova A, and Hoogenraad CC (2017). MAP2 defines a pre-axonal filtering zone to regulate KIF1- versus KIF5-dependent cargo transport in sensory neurons. Neuron 94, 347–362. [PubMed: 28426968]

Hall DH, and Hedgecock EM (1991). Kinesin-related gene unc-104 is required for axonal transport of synaptic vesicles in C. elegans. Cell 65, 837–847. [PubMed: 1710172]

Jin Y, and Garner CC (2008). Molecular mechanisms of presynaptic differentiation. Annu. Rev. Cell Dev. Biol 24, 237–262. [PubMed: 18588488]

Kaeser PS, Deng L, Wang Y, Dulubova I, Liu X, Rizo J, and Südhof TC (2011). RIM proteins tether Ca2+ channels to presynaptic active zones via a direct PDZ-domain interaction. Cell 144, 282–295. [PubMed: 21241895]

Kevenaar JT, and Hoogenraad CC (2015). The axonal cytoskeleton: from organization to function. Front. Mol. Neurosci 8, 44. [PubMed: 26321907]

Kittel RJ, Wichmann C, Rasse TM, Fouquet W, Schmidt M, Schmid A, Wagh DA, Pawlu C, Kellner RR, Willig KI, et al. (2006). Bruchpilot promotes active zone assembly, Ca2+ channel clustering, and vesicle release. Science 312, 1051–1054. [PubMed: 16614170]

Kittelmann M, Hegermann J, Goncharov A, Taru H, Ellisman MH, Richmond JE, Jin Y, and Eimer S (2013). Liprin-α/SYD-2 determines the size of dense projections in presynaptic active zones in *C. elegans*. J. Cell Biol 203, 849–863. [PubMed: 24322429]

Klassen MP, Wu YE, Maeder CI, Nakae I, Cueva JG, Lehrman EK, Tada M, Gengyo-Ando K, Wang GJ, Goodman M, et al. (2010). An Arf-like small G protein, ARL-8, promotes the axonal transport of presynaptic cargoes by suppressing vesicle aggregation. Neuron 66, 710–723. [PubMed: 20547129]

Li J, Zhang YV, Asghari Adib E, Stanchev DT, Xiong X, Klinedinst S, Soppina P, Jahn TR, Hume RI, Rasse TM, and Collins CA (2017). Restraint of presynaptic protein levels by Wnd/DLK signaling mediates synaptic defects associated with the kinesin-3 motor Unc-104. eLife 6, e24271. [PubMed: 28925357]

Liu C, Kershberg L, Wang J, Schneeberger S, and Kaeser PS (2018). Dopamine secretion is mediated by sparse active zone-like release sites. Cell 172, 706–718. [PubMed: 29398114]

Maas C, Torres VI, Altrock WD, Leal-Ortiz S, Wagh D, Terry-Lorenzo RT, Fejtova A, Gundelfinger ED, Ziv NE, and Garner CC (2012). Formation of Golgi-derived active zone precursor vesicles. J. Neurosci 32, 11095–11108. [PubMed: 22875941]

Maeder CI, Shen K, and Hoogenraad CC (2014). Axon and dendritic trafficking. Curr. Opin. Neurobiol 27, 165–170. [PubMed: 24762653]

Niwa S, Lipton DM, Morikawa M, Zhao C, Hirokawa N, Lu H, and Shen K (2016). Autoinhibition of a neuronal kinesin UNC-104/KIF1A regulates the size and density of synapses. Cell Rep. 16, 2129–2141. [PubMed: 27524618]

Okada Y, Yamazaki H, Sekine-Aizawa Y, and Hirokawa N (1995). The neuron-specific kinesin superfamily protein KIF1A is a unique monomeric motor for anterograde axonal transport of synaptic vesicle precursors. Cell 81, 769–780. [PubMed: 7539720]

Pack-Chung E, Kurshan PT, Dickman DK, and Schwarz TL (2007). A Drosophila kinesin required for synaptic bouton formation and synaptic vesicle transport. Nat. Neurosci 10, 980–989. [PubMed: 17643120]

Patel MR, Lehrman EK, Poon VY, Crump JG, Zhen M, Bargmann CI, and Shen K (2006). Hierarchical assembly of presynaptic components in defined C. elegans synapses. Nat. Neurosci 9, 1488–1498. [PubMed: 17115039]

Petzoldt AG, Lützkendorf J, and Sigrist SJ (2016). Mechanisms controlling assembly and plasticity of presynaptic active zone scaffolds. Curr. Opin. Neurobiol 39, 69–76. [PubMed: 27131423]

Sabo SL, Gomes RA, and McAllister AK (2006). Formation of presynaptic terminals at predefined sites along axons. J. Neurosci 26, 10813–10825. [PubMed: 17050720]

Sawin ER, Ranganathan R, and Horvitz HR (2000). *C. elegans* locomotory rate is modulated by the environment through a dopaminergic pathway and by experience through a serotonergic pathway. Neuron 26, 619–631. [PubMed: 10896158]

Schwartz ML, and Jorgensen EM (2016). SapTrap, a toolkit for highthroughput CRISPR/Cas9 gene modification in *Caenorhabditis elegans*. Genetics 202, 1277–1288. [PubMed: 26837755]

Scott DA, Das U, Tang Y, and Roy S (2011). Mechanistic logic underlying the axonal transport of cytosolic proteins. Neuron 70, 441–454. [PubMed: 21555071]

Shapira M, Zhai RG, Dresbach T, Bresler T, Torres VI, Gundelfinger ED, Ziv NE, and Garner CC (2003). Unitary assembly of presynaptic active zones from Piccolo-Bassoon transport vesicles. Neuron 38, 237–252. [PubMed: 12718858]

Südhof TC (2012). The presynaptic active zone. Neuron 75, 11–25. [PubMed: 22794257]

Südhof TC (2013). Neurotransmitter release: the last millisecond in the life of a synaptic vesicle. Neuron 80, 675–690. [PubMed: 24183019]

Sulzer D, Cragg SJ, and Rice ME (2016). Striatal dopamine neurotransmission: regulation of release and uptake. Basal Ganglia 6, 123–148. [PubMed: 27141430]

Tang Y, Scott D, Das U, Gitler D, Ganguly A, and Roy S (2013). Fast vesicle transport is required for the slow axonal transport of synapsin. J. Neurosci 33, 15362–15375. [PubMed: 24068803]

Tao-Cheng J-H (2007). Ultrastructural localization of active zone and synaptic vesicle proteins in a preassembled multi-vesicle transport aggregate. Neuroscience 150, 575–584. [PubMed: 17977664]

Trudeau L-E, Hnasko TS, Wallén-Mackenzie A, Morales M, Rayport S, and Sulzer D (2014). The multilingual nature of dopamine neurons. Prog. Brain Res 211, 141–164. [PubMed: 24968779]

Wang Y, Liu X, Biederer T, and Südhof TC (2002). A family of RIM-binding proteins regulated by alternative splicing: Implications for the genesis of synaptic active zones. Proc. Natl. Acad. Sci. USA 99, 14464–14469. [PubMed: 12391317]

Wong MY, Zhou C, Shakiryanova D, Lloyd TE, Deitcher DL, and Levitan ES (2012). Neuropeptide delivery to synapses by long-range vesicle circulation and sporadic capture. Cell 148, 1029–1038. [PubMed: 22385966]

Wu YE, Huo L, Maeder CI, Feng W, and Shen K (2013). The balance between capture and dissociation of presynaptic proteins controls the spatial distribution of synapses. Neuron 78, 994–1011. [PubMed: 23727120]

Xuan Z, Manning L, Nelson J, Richmond JE, Colón-Ramos DA, Shen K, and Kurshan PT (2017). Clarinet (CLA-1), a novel active zone protein required for synaptic vesicle clustering and release. eLife 6, e29276. [PubMed: 29160205]

Yogev S, Cooper R, Fetter R, Horowitz M, and Shen K (2016). Microtubule organization determines axonal transport dynamics. Neuron 92, 449–460. [PubMed: 27764672]

Zhai RG, Vardinon-Friedman H, Cases-Langhoff C, Becker B, Gundelfinger ED, Ziv NE, and Garner CC (2001). Assembling the presynaptic active zone: a characterization of an active one precursor vesicle. Neuron 29, 131–143. [PubMed: 11182086]

Zhen M, and Jin Y (1999). The liprin protein SYD-2 regulates the differentiation of presynaptic termini in C. elegans. Nature 401, 371–375. [PubMed: 10517634]

Ziv NE, and Garner CC (2004). Cellular and molecular mechanisms of presynaptic assembly. Nat. Rev. Neurosci 5, 385–399. [PubMed: 15100721]

Highlights

- Rapid *in vivo* formation of presynaptic specializations
- Synaptic vesicle precursors (SVPs) and active zone proteins coalesce simultaneously
- Regulation of Kinesin-3 influences aggregation of SVPs

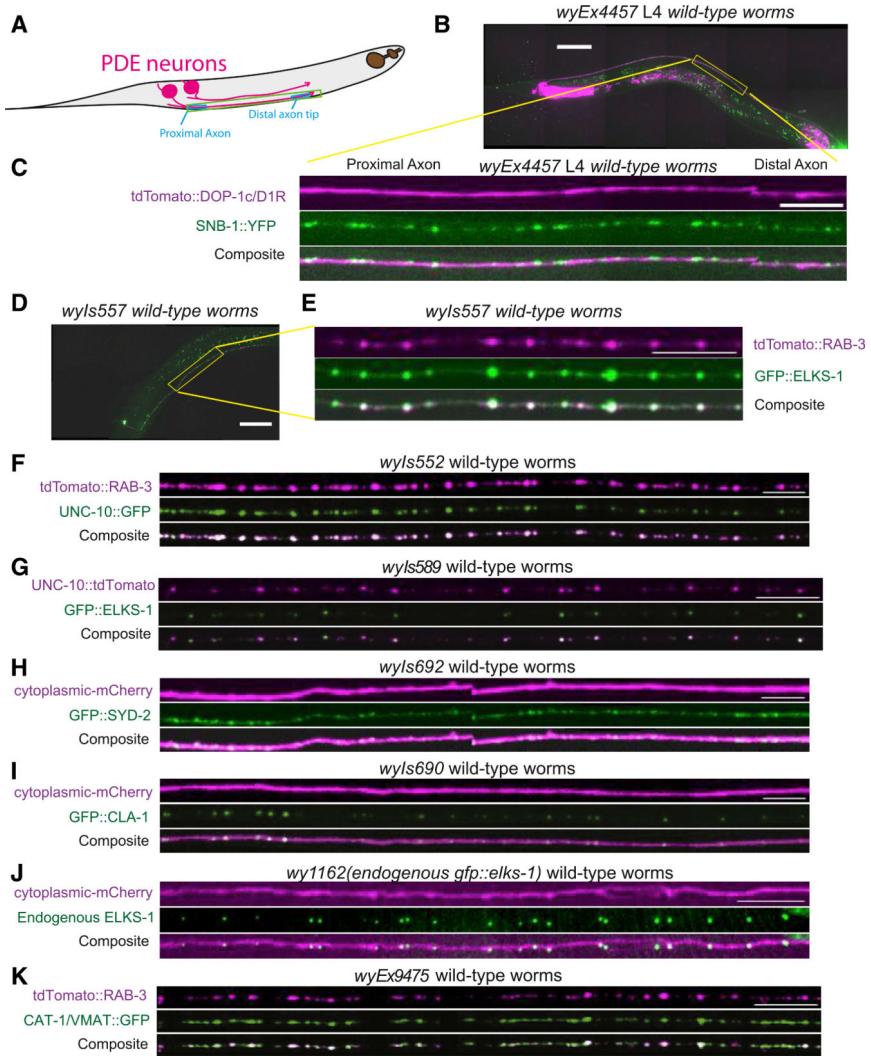

Figure 1. Dopaminergic Presynaptic Specializations in PDE Neurons Contain Active Zone Proteins

(A) Model of two PDE neurons with axons extending anteriorly along the ventral nerve cord.

(B) Micrograph of *wyEx4457* L4 wild-type worm showing expression of tdTomato:DOP-1c using DVA-specific promoter and Pdat-1::SNB-1::GFP. Scale bar, 50 μm.

(C) Inset in (B). Scale bar, 10 μm.

(D) Micrograph of *wyIs557* L4 wild-type worms, showing Pdat-1::tdTomato::RAB-3 and Pdat-1:: GFP::ELKS-1. Scale bar, 50 μm.

(E) Inset in (D). Scale bar, 10 μm.

(F–K) Axon insets similar to (C) and (E) depicting the following Pdat-1-driven protein-XFP fusion constructs in PDE axons. Strain names are indicated on top of the micrographs, and expressed fusion proteins are to the left. Scale bars, 10 μm.

(F)tdTomato::RAB-3 and UNC-10::GFP.

(G)UNC-10::tdTomato and GFP::ELKS-1.

(H)Cytoplasmic::mCherry and GFP::SYD-2.

(I)Cytoplasmic::mCherry and GFP::Cla-1.
(J) GFP::ELKS-1 endogenously tagged and cytoplasmic mCherry exogenously expressed exclusively in Pdat-1+ neurons in *wy1162*; *wyIs834* worms.
(K) tdTomato::RAB-3 and CAT-1/VMAT::GFP.

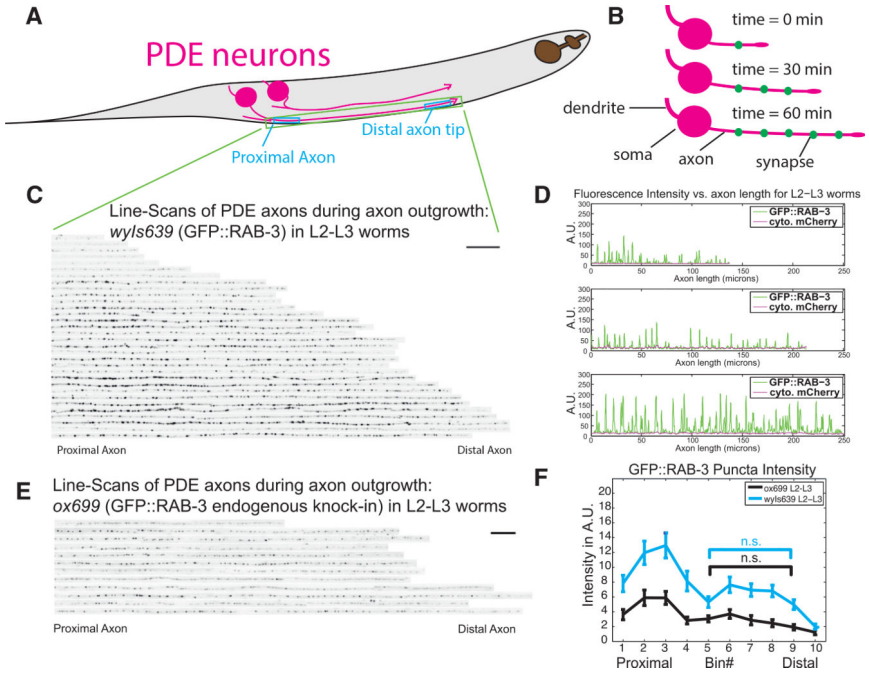

Figure 2. Synaptic Vesicle Precursors Rapidly Coalesce into Puncta behind the Growth Cone

(A) Model of PDE axons showing proximal and distal axon segments.

(B) Model of PDE axon outgrowth over time.

(C) Line scans showing the puncta intensity of GFP::RAB-3, a synaptic vesicle precursor marker, along axons from many *wyIs639* wild-type worms stacked together. Axons ordered by length of outgrowing PDE axon. Scale bar, 20 μm.

(D) Plot profiles of GFP::RAB-3 and cytoplasmic-mCherry fluorescence intensity along three representative axons.

(E) Line scans of GFP::RAB-3 endogenously tagged in *ox699* worms with dopamine neuron Flippase (Pdat-1::FLP). Scale bar, 20 μm.

(F) Mean GFP::RAB-3 intensity distribution of thresholded puncta in ox699 worms in 10 proximal-distal bins (1 = proximal, 10 = distal) along PDE axons. Significance values are computed within a genotype cohort. Means and SEMs are shown. *p < 0.05; **p < 0.01; ***p < 0.001.

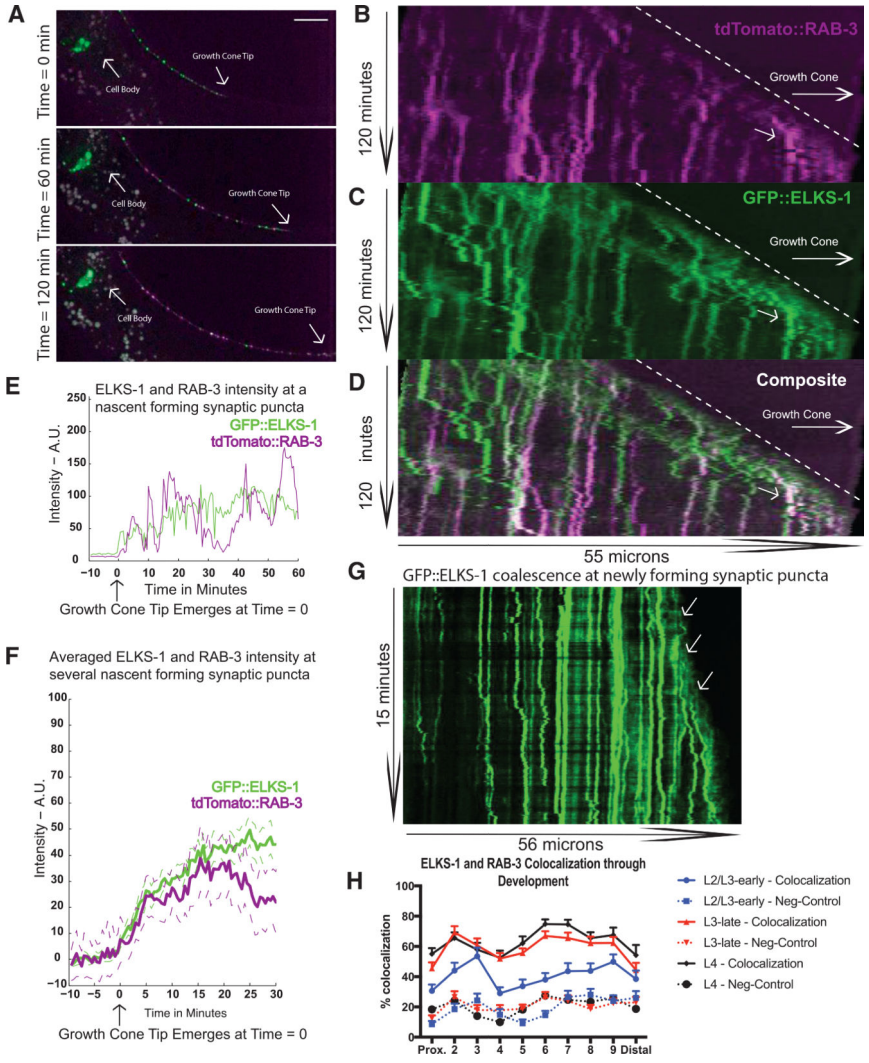

Figure 3. Synaptic Vesicle Precursors and Active Zone Proteins Coalesce Simultaneously and Rapidly behind Outgrowing PDE Axon Tip

(A) Micrographs of tdTomato::RAB-3, a synaptic vesicle precursor (SVP) marker (magenta) and GFP::ELKS-1, an active zone (AZ) protein (green) in a PDE cell body and axon in *wyIs557* wild-type worms at selected time points during axon outgrowth. Scale bar, 10 μm.

(B and C) Kymographs generated from movies taken of tdTomato::RAB-3 (B) and GFP::ELKS-1 (C) fluorescence intensity along an outgrowing PDE axon from a single *wyIs557* wild-type worm.

(D)Composite of (B) and (C).

(E) Fluorescence intensity of GFP::ELKS-1 and tdTomato::RAB-3 at a single coalescing puncta over time. The region of interest (ROI) was selected by tracing backward in time at the axonal site of a stable GFP::ELKS-1 puncta at the end of the movie, accounting for slight puncta movements.

(F) Mean of individual punctum coalescence traces of GFP::ELKS-1 (green) and tdTomato::RAB-3 (magenta). Dashed lines represent ± SEMs.

(G) Kymograph of ELKS-1 fluorescence intensity at higher temporal resolution (image taken every 2.5 s). Arrows indicate puncta formation events.
(H) Percentage of colocalization between thresholded ELKS-1 and RAB-3 puncta in *wyIs557* wildtype worms as a function of developmental stage. For negative controls, RAB-3 images were horizontally shifted and the percentage of overlap was recalculated. Means and SEMs are shown. Number of worms: L2 and early-L3 worms, n = 37; late-L3 worms, n = 33; L4 worms, n = 21.

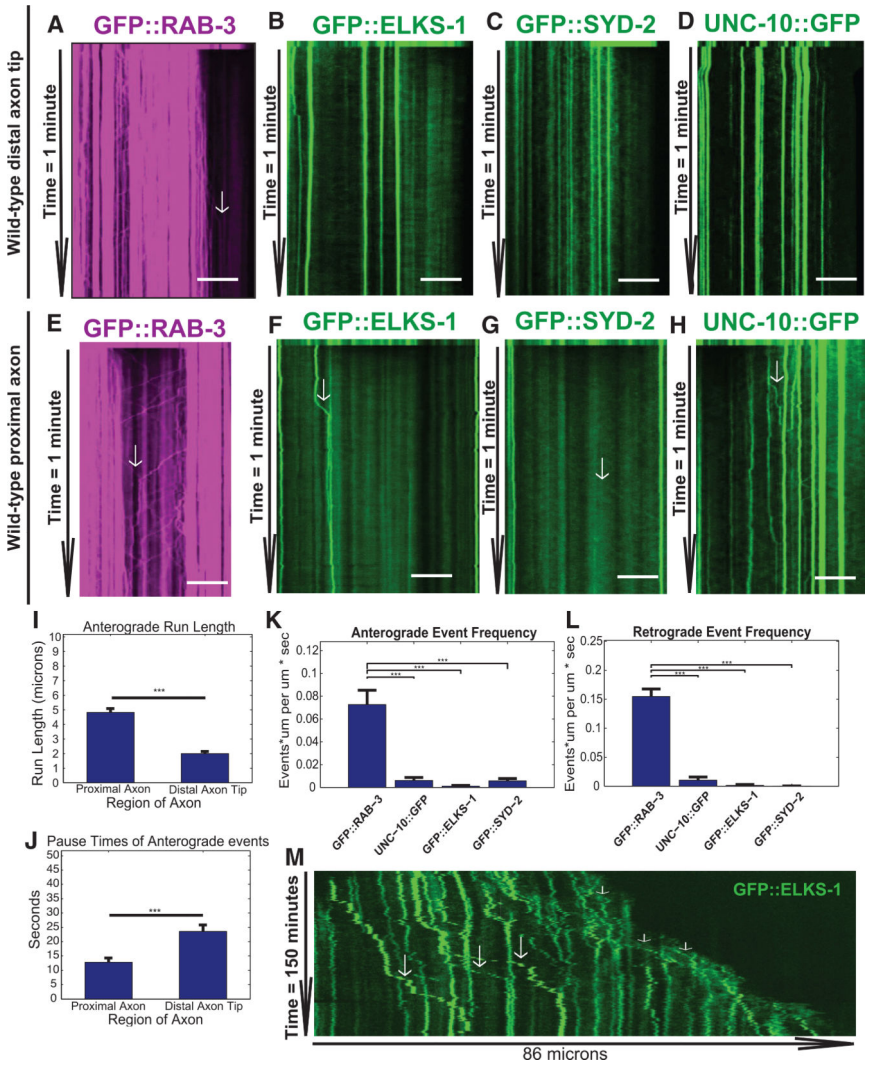

Figure 4. AZ Proteins and Synaptic Vesicle Precursors Exhibit Different Transport Dynamics along the Axon

(A–D) Kymographs from movies of fluorescence intensity of SVP marker RAB-3 (A) and AZ proteins (B–D) in the PDE axon tip in L2–L3 worms after the first photo-bleaching axon tip. Proteins and worm strains (in parentheses) are (A) GFP::RAB-3 (*wyIs639*), (B) GFP::ELKS-1 (*wyIs557*), (C) GFP:: SYD-2 (*wyIs692*), and (D) UNC-10::GFP (*wyIs552*). Scale bar, 5 μm. Arrows indicate transport events. Anterograde events are those traveling to the right, and retrograde events are traveling to the left. The frame rate of movies is 7.5 images per second. The first 10 rows of the kymograph represent the prebleach image. (E–H) Same as (A)–(D), except kymographs are taken from the PDE proximal axon. Proteins and worm strains (in parentheses) are (E) GFP::RAB-3 (*wyIs639*), (F) GFP::ELKS-1 (*wyIs557*), (G) GFP:: SYD-2 (*wyIs692*), and (H) UNC-10::GFP (*wyIs552*). (I–L) Mean anterograde event run length (I) and pause times (J) in proximal versus distal regions of PDE axon. Event numbers: (I) proximal axon, n = 150; distal axon, n = 62; (J) proximal axon, n = 104; distal axon, n = 59. (K and L) Anterograde (K) and retrograde (L) event frequency. Frequency = (sum of total run lengths) / (total distance imaged * time). n =

number of kymographs imaged: GFP::RAB-3, n = 17; UNC-10::GFP, n = 34; GFP::ELKS-1, n = 23; GFP::SYD-2, n = 29. (I–L) Means and SEMs are shown. *$p < 0.05$; **$p < 0.01$; ***$p < 0.001$.

(M) Long-term kymographs of GFP::ELKS-1 similar to Figure 3C. Long and short arrows indicate ELKS-1 movements along the mature axon and behind the growth cone, respectively.

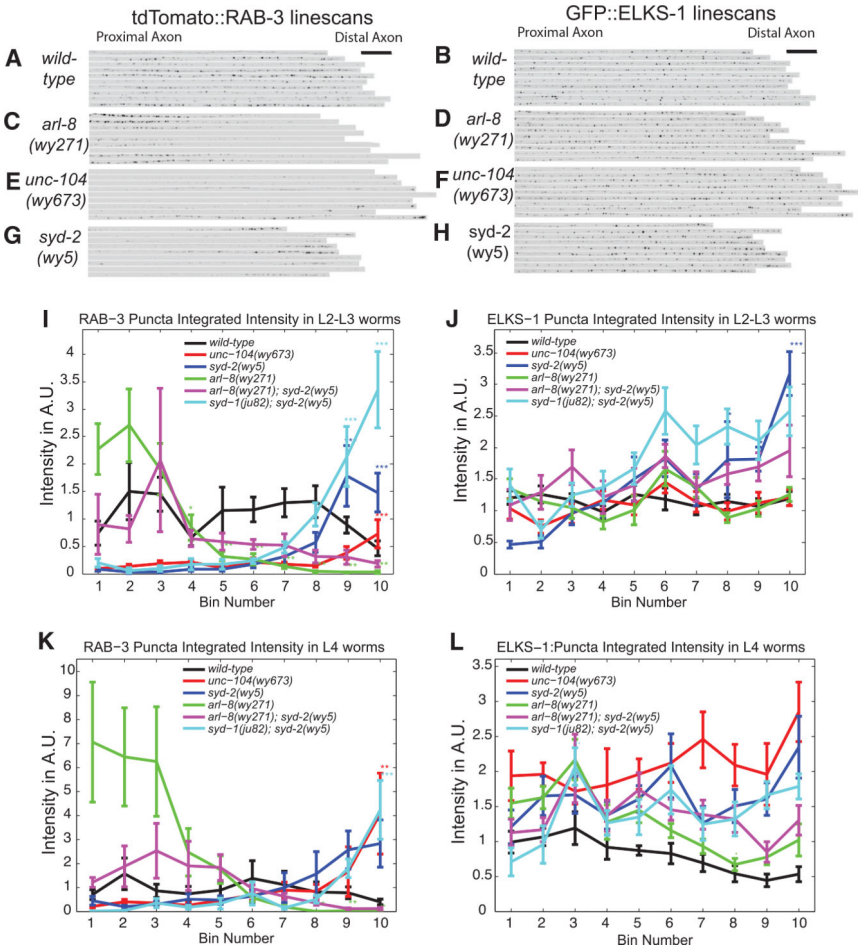

Figure 5. Balance between Transport and Aggregation Positions Synaptic Vesicle Clusters at an Early Stage of Synapse Formation

(A–J) Line scans of tdTomato::RAB-3 (A, C, E, and G) and GFP::ELKS-1 (B, D, F, and H) intensity in wyIs557 L2–L3 worms for the following genotypes: (A and B) wild-type, (C and D) arl-8(wy271), (E and F) unc-104(673), and (G and H) syd-2(wy5). Scale bars for (A)–(H) in (A) and (B). Scalebar, 20 μm. (B), (D), (F), and (H) are images from the same *wyIs557* L2–L3 worms as used in (A), (C), (E), and (G), respectively.

(I and J) Mean tdTomato::RAB-3 (I) and GFP::ELKS1 (J) puncta intensity plots across 10 proximal-distal bins in L2–L3 worms of the indicated genotypes. Number of worms: wild-type, n = 23; *unc104(wy673)*, n = 25; *syd-2(wy5)*, n = 15; *arl-8(wy271)*, n = 20; *arl-8(wy271); syd-2(wy5)*, n = 7; *syd-1(ju82); syd-2(wy5)*, n = 17.

(K and L) Mean tdTomato::RAB-3 (K) and GFP::ELKS-1 (L) puncta intensity plots across 10 proximal-distal bins in L4 worms of the indicated genotypes. Number of worms: wild-type, n = 17; *unc-104(wy673)*, n = 9; *syd-2(wy5)*, n = 9; *arl8(wy271)*, n = 10; *arl-8(wy271); syd-2(wy5)*, n = 12; *syd-1(ju82); syd-2(wy5)*, n = 5.

(I–L) Line plots of integrated puncta intensity per bin in *wyIs557* worms for the following genotypes: wildtype, *unc-104(wy673)*, *syd-2(wy5)*, *arl-8(wy271)*, *arl8(wy271); syd-2(wy5)*, and *syd-1(ju82); syd-2(wy5)*. Significance values are computed only within a genotype cohort. Means and SEMs are shown. *p < 0.05; **p < 0.01; ***p < 0.001.

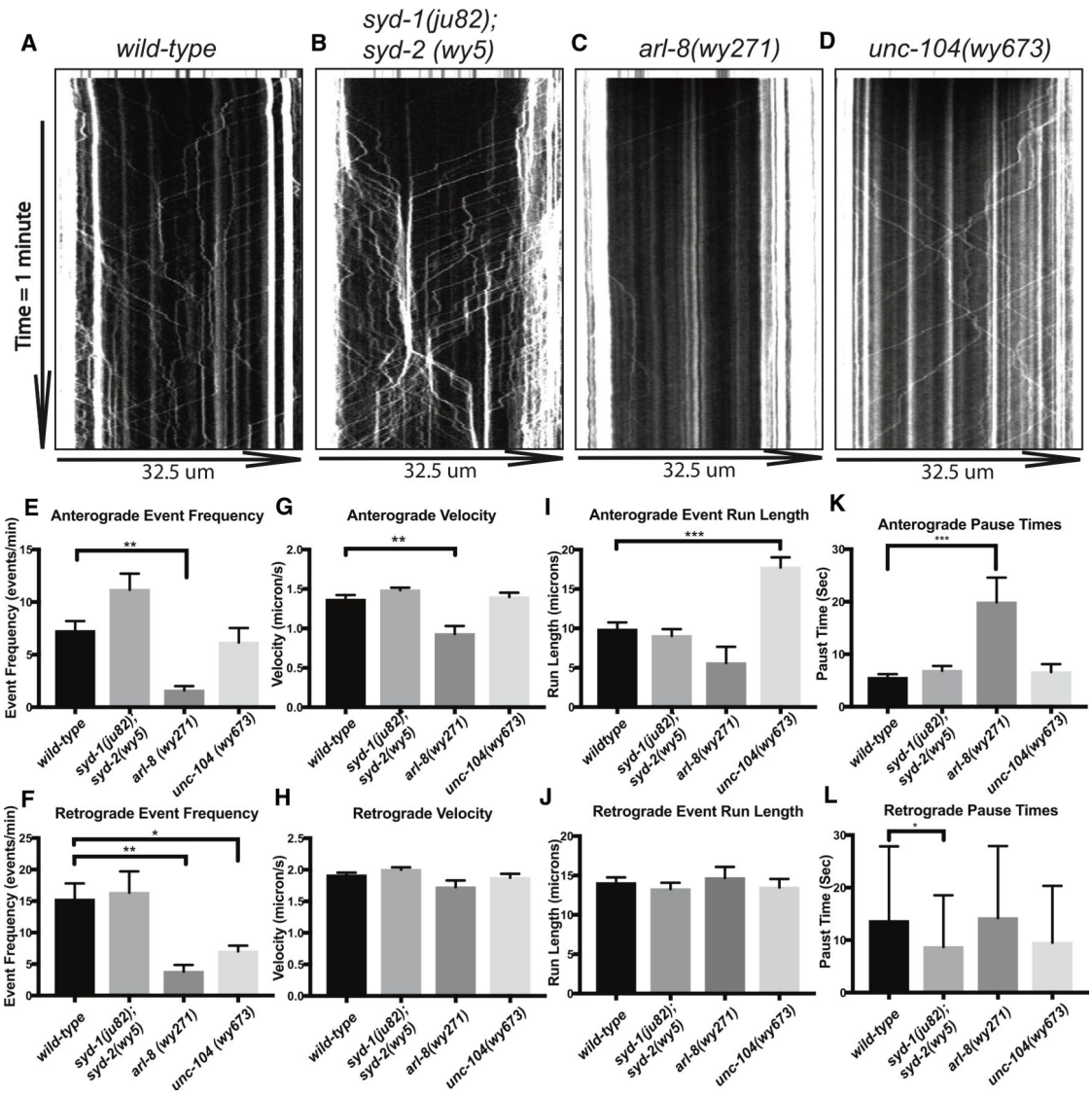

Figure 6. UNC-104/Kinesin-3 Activation State Dynamically Regulates Synaptic Vesicle Precursor Transport

(A–D) Kymographs from movies of GFP::RAB-3 fluorescence intensity along the axon in proximal PDE axon in wyIs639 L3 worms (depicted in Figure 1A), similar to Figure 4: (A) wild-type, (B) *syd-1(ju82); syd-2(wy5)*, (C) *arl-8(wy271)*, and (D) *unc-104(wy673)*. The movie frame rate is 7.5 images per second. The first 10 rows of the kymograph are pre-bleach images.

(E and F) Anterograde (E) and retrograde (F) transport event frequencies, measured as the mean number of events observed per 1-min kymograph. wild-type, n = 8; *syd-1(ju82); syd-2(wy5)*, n = 6; *arl-8(wy271)*, n = 5; *unc-104(wy673)*, n = 8.

(G–J) Number of events below.

(G and H) Anterograde (G) and retrograde (H) velocities in micrometers per second.

(I and J) Anterograde (I) and retrograde (J) run lengths, in micrometers traveled from entering the bleached imaging window until pausing. (G and I) Anterograde event numbers:

wild-type, n = 59; *syd-1(ju82)*; *syd-2(wy5)*, n = 67; *arl-8(wy271)*, n = 7; *unc-104(wy673)*, n = 43.

(H and J) Retrograde event numbers: wild-type, n = 122; *syd-1(ju82)*; *syd-2(wy5)*, n = 98; *arl-8(wy271)*, n = 19; *unc-104(wy673)*, n = 49.

(K and L) Mean pause times for anterograde (K) and retrograde (L) transport events that pause during transport. Number of events below. (K) Anterograde pause time event numbers: wild-type, n = 87; *syd-1(ju82)*; *syd-2(wy5)*, n = 100; *arl-8(wy271)*, n = 10; *unc-104(wy673)*, n = 39. (L) Retrograde pause time numbers: wild-type, n = 112; *syd-1(ju82)*; *syd-2(wy5)*, n = 117; *arl-8(wy271)*, n = 16; *unc-104(wy673)*, n = 52.

(E–L) *p < 0.05; **p < 0.01; ***p < 0.001.

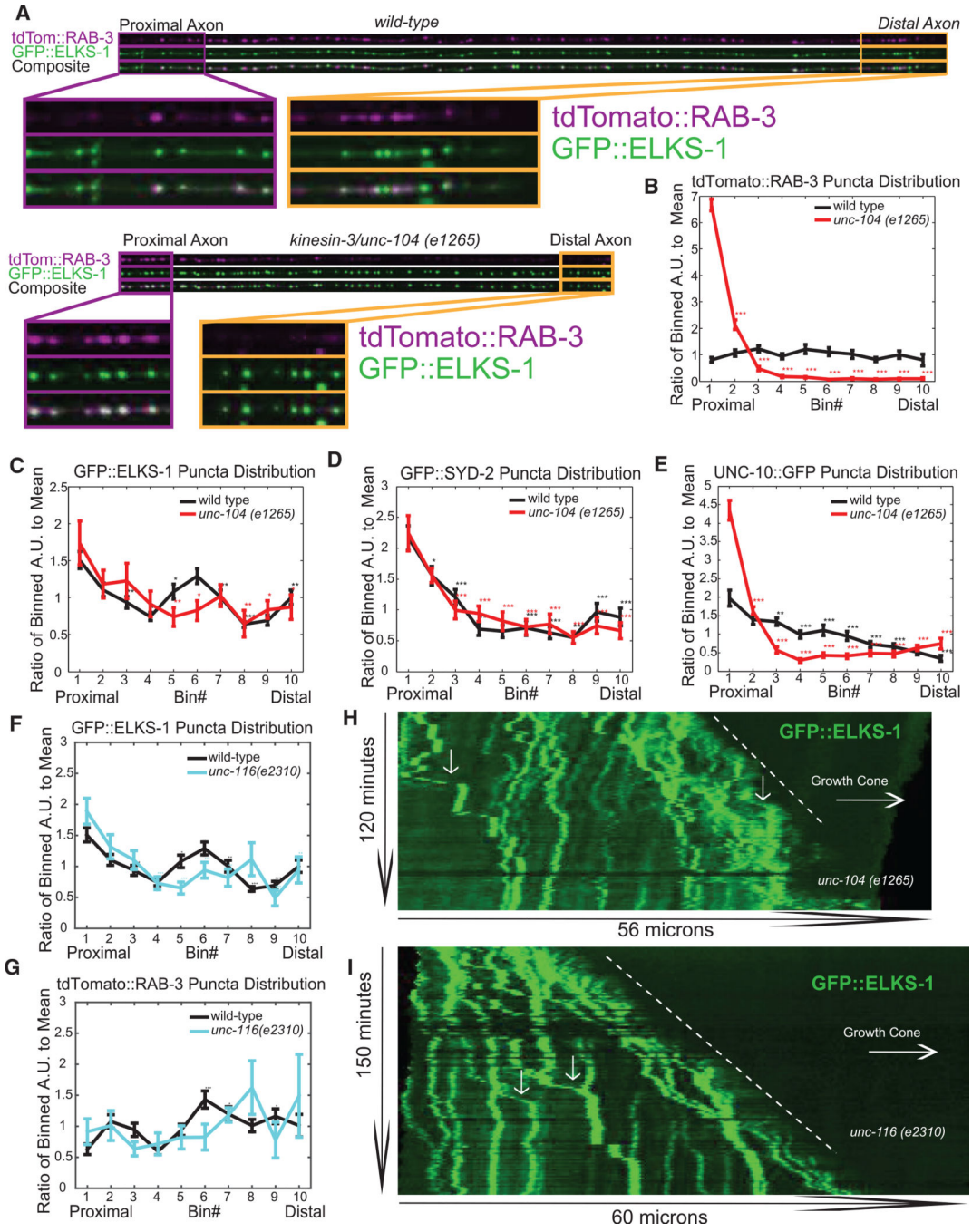

Figure 7. AZ Protein Transport Is Mostly Independent of UNC-104/Kinesin-3 and UNC-116/ Kinesin-1

(A) Line scans of tdTomato::RAB-3 and GFP::ELKS-1 fluorescence intensity in wild-type and *unc-104(e1265)* mutant worms. Inset scale: wild-type = 26 μm, *unc104(e1265)* = 24 μm. (B–E) Distribution of mean (B) tdTomato::RAB-3, (C) GFP::ELKS-1, (D) GFP::SYD-2, and (E) UNC-10::GFP puncta intensity in 10 proximal-distal (1 = proximal, 10 = distal) bins along the PDE axon in both wild-type and *unc-104(e1265)* mutants. Number of axons: (B) tdTomato::RAB-3 (*wyIs552*): wild-type, n = 23; *unc-104*, n = 25. (C) GFP::ELKS-1 (*wyIs557*): wild-type, n = 34; *unc-104*, n = 12. (D) GFP::SYD-2 (*wyIs692*): wild-type, n =

38; *unc-104*, n = 12. (E) UNC-10::GFP (*wyIs552*): wild-type, n = 23; *unc-104*, n = 25. Significance computed between the first bin and all subsequent bins within a single genotype cohort. Means and SEMs are shown. *p < 0.05; **p < 0.01; ***p < 0.001. (F and G) Distribution of mean (F) ELKS-1 and (G) RAB-3 puncta intensity in wild-type and *unc-116*(*e2310*) mutant axons, similar to (B)–(E). wild-type, n=34; *unc-116*, n=8. (H and I) Kymographs of GFP::ELKS-1 intensity similar to Figure 3C, taken in *unc-104*(*e1265*) worms (H) and *unc-116*(*e2310*) worms (I). Arrows indicate slow anterograde ELKS-1 movements.